Ion energy distributions in a pulsed, electron beam-generated plasma

S. G. Walton,[a),b)] D. Leonhardt, D. D. Blackwell,[b)] R. F. Fernsler, D. P. Murphy, and R. A. Meger
Plasma Physics Division, U.S. Naval Research Laboratory, Washington, DC 20375

(Received 9 October 2000; accepted 4 December 2000)

In this work, we investigate the ion flux at a grounded electrode located adjacent to a pulsed, argon plasma generated by a high-energy electron beam. The plasmas, produced in 100 mTorr, are characterized by high plasma densities ($>10^{11}\,\mathrm{cm}^{-3}$) and low electron temperatures (<1.5 eV). An energy selective mass spectrometer was used to measure temporally resolved ion kinetic-energy distributions at the electrode surface. In addition, ion energy distributions are presented for various electrode locations. The ion energy distributions correlate well with Langmuir probe measurements of the plasma potential. © *2001 American Vacuum Society.* [DOI: 10.1116/1.1345901]

I. INTRODUCTION

The Naval Research Laboratory (NRL) has developed a different type of plasma reactor, coined a large area plasma processing system (LAPPS). LAPPS employs a magnetically confined sheet of high-energy electrons to ionize a background gas and thus generate a plasma. Electron beams are very efficient plasma sources and have been shown to produce high-density, low electron temperature plasmas with high uniformity.[1,2] Given these attributes, we set out to develop a 1 m^2 plasma source for materials' processing over large areas. Other unique features of electron beam-generated plasmas make them attractive as processing sources.[3,4] For example, such sources are found to have an increased rate of radical production whose flux to the substrate surface is beneficial to etching. Of particular interest to these investigations is that plasma production is decoupled from the reactor geometry, which allows independent biasing and positioning of electrode (or substrate) surfaces. Like other high-density plasma sources used in processing, the incident ion energy at the substrate surface may be controlled with an applied bias. Independence of the electrode location allows additional control over the composition of the flux to the surface: Ions diffusing toward the electrode could be converted to other ion species via charge exchange collisions with background species.

In this work, we investigate the ion flux incident to a grounded electrode located adjacent to a pulsed, electron beam-generated plasma in argon. Mass and time resolved ion energy distributions are measured as a function of electrode location. We compare the results with probe measurements used to characterize the plasma.[5]

II. EXPERIMENTAL METHODS

The experimental apparatus is schematically represented in Fig. 1. The discharge reactor is a cylindrical aluminum chamber with an inner diameter of 50 cm and a length of 60 cm. Helmholtz coils, attached to the chamber, provide 150 G along the axis of the chamber. In the region between the coils and out to a radius of 15 cm, the fluctuations in field strength are less than 10%.

The base pressure of the reactor is 1×10^{-5} Torr. High purity (99.999%) argon gas is introduced through mass flow controllers and pumped out through a 1.5 in. metal seal valve by a turbomolecular drag pump. The operating pressure is achieved by varying the conductance through the valve. The flow is typically held between 5 and 10 sccm to achieve operating pressures between 50 and 100 mTorr. For all measurements in this work, the operating pressure is held constant at 100 mTorr.

The electron beam is produced by a long hollow-cathode discharge.[1] The cathode is driven by a high negative voltage pulse and generates an electron beam commensurate to the applied voltage. The emerging electron beam, confined by the magnetic field, is passed through a slot in a grounded anode located 5 cm downstream from the hollow cathode and then terminated at a grounded beam dump. Between the anode and dump, the electron beam ionizes the background gas to form a plasma and defines the source region. The dimensions of the plasma source, dictated by the beam dimensions, are set by the slot size and the distance between the anode and beam dump. In this case, the plasma source is 24 cm wide×37 cm long×1 cm thick. For the experiments herein, the cathode is driven to -1.0 kV for 1.0 ms at a frequency of 33 Hz. To monitor the discharge, the currents to the cathode, anode, and beam dump are measured with a Pearson coil (Fig. 2). Because of design limitations, the hollow cathode is located 8.0 cm radially from the axis of the reactor. Even so, the magnetic field is still within 10% of its maximum value over the entire discharge.

Ion flux and energy distributions are measured with a Hiden EQP 300 plasma probe (Fig. 1) that consists of an electrostatic ion-energy analyzer (ESA) in series with a quadrupole mass spectrometer (QMS). The probe is inserted from the side of the chamber with the probe axis perpendicular to the plasma sheet. The end of the probe is fitted with a stainless steel electrode. Ions incident to the electrode enter the probe through a 100 μm diam aperture in the center of the electrode. Alternatively, the probe can function as a re-

[a)]Electronic mail: sgwalton@ccs.nrl.navy.mil
[b)]NRL/NRC postdoctoral research associate.

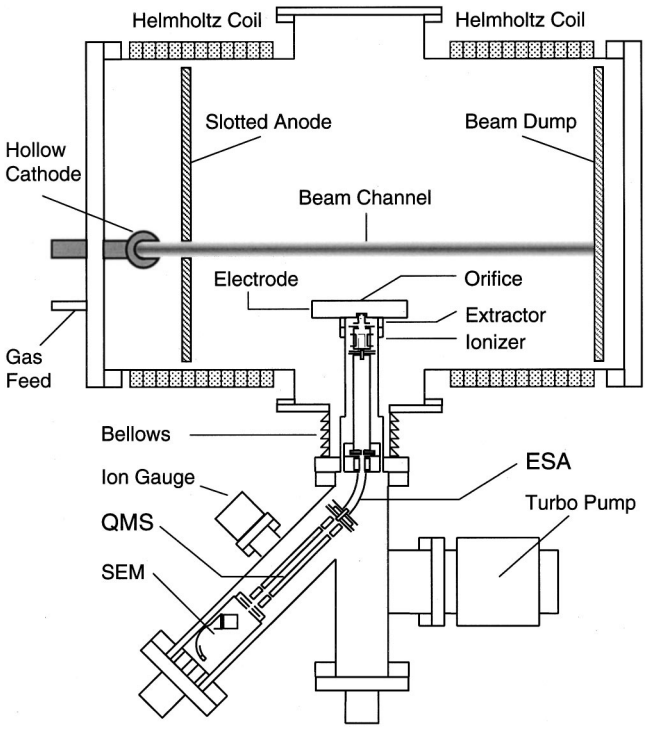

FIG. 1. Schematic diagram of the reactor and the plasma probe (not drawn to scale). Only the cross-section of the hollow cathode and discharge are shown (the third dimension extends into the page). The plasma probe consists of an electrostatic energy analyzer in series with a quadrupole mass spectrometer. The ionizer at the electrode end of the probe allows the probe to be operated as a residual gas analyzer. A bellows connects the probe to the reactor so that the source–electrode separation may be adjusted.

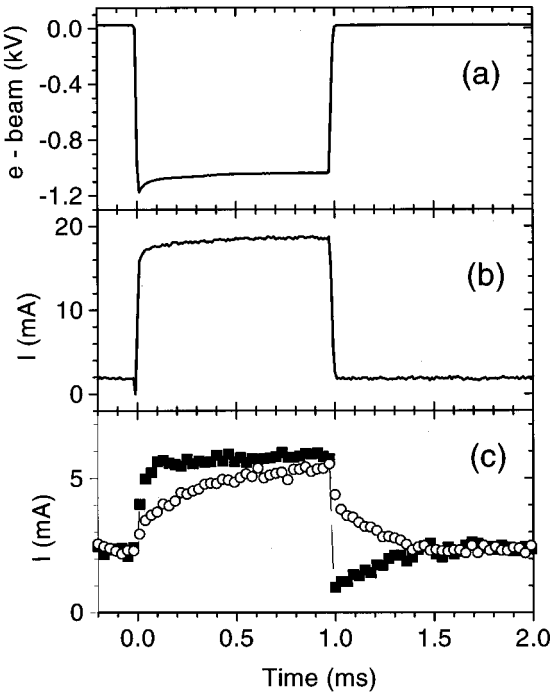

FIG. 2. Current and voltage signals used to monitor the electron beam-generated plasma in argon. The electron beam pulse duration is 1.0 ms and the repetition rate is 33 Hz. Shown are (a) the voltage across the anode–cathode gap, (b) the current supplied to the hollow cathode, and (c) the currents measured at the slotted anode (squares) and the beam dump (circles). For all measurements in this work, $t=0$ is defined by the front of the signals shown.

sidual gas analyzer (RGA). In this mode, neutrals diffusing through the orifice are ionized via an internal electron source.

Extraction optics, located adjacent to the orifice, accelerate ions into a drift region prior to entering the ESA and the QMS. The instrument is designed such that ions are first energy selected by the ESA, then mass selected by the QMS, and finally detected by a channeltron secondary-electron multiplier (SEM). All ions transit the ESA, a 45° sector-field energy analyzer, at a fixed transmission energy independent of their initial kinetic energy at the electrode surface. The transmission energy determines the full width at half maximum, ΔE. For the measurements here, the ESA was operated at three transmission energies which correspond to $\Delta E = 1.0$, 0.5, and 0.3 eV. Hence for a measured energy, E, the ion flux corresponds to ions with energies in the range of $E \pm \Delta E/2$.

The QMS employs a time-varying electric quadrupole field to separate ions according to their mass-to-charge ratio. The transmission efficiency of the QMS decreases with increasing mass, however for the principal mass range of interest here (1–50 amu), the mass dependence does not significantly affect the transmission and so no attempt was made to adjust the measured intensities.

The relationship between the absolute flux at the electrode surface and the signal intensity is determined by the fraction of incident ions that reach the SEM and the response of the SEM. The EQP has not been calibrated for absolute intensities and so it is not possible to determine absolute fluxes. For this reason, the signal intensities are reported in arbitrary units. However, it is reasonable to compare relative signal intensities. In order to do this, the probe settings are determined by optimizing the Ar^+ signal for a fixed set of experimental parameters.

Differential pumping keeps the pressure inside the probe below 2×10^{-6} Torr during the measurements, which allows for nearly collision-free transit of ions in the probe. Given the experimental parameters, the number of ions that reach the detector without undergoing collisions may be estimated.[6,7] For ion energies of 1 eV and a plasma pressure of 100 mTorr in the reactor, approximately 87% of the ions will transit the probe without experiencing a collision.

Time-resolved measurements are achieved by gating the output of the channeltron with a pulse of a given width and delay (with respect to the front of the hollow-cathode pulse) such that only ions arriving at the channeltron during the gating pulse will be counted. Energy distributions need to be accumulated over several hundred pulses to achieve a reasonable signal-to-noise ratio. Alternatively, the output from the channeltron can be monitored in real time by a gated pulse counter. The counter gate width can be set and scanned over the entire time range of interest. This mode allows much shorter data acquisition times, especially when high temporal resolution (narrow time window) is required.

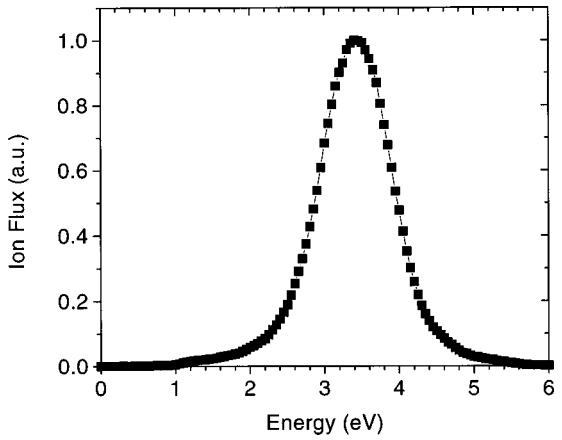

FIG. 3. Temporally resolved kinetic-energy distribution of Ar^+ incident to a grounded electrode surface located 1.0 cm from the edge of the electron beam. The ions are sampled through a small orifice (100 μm diameter) located in the center of the electrode. The discharge is produced the same as in Fig. 2 and the ion flux is measured during a time window between 200 μs and 1.0 ms. The energy uncertainty is ± 0.15 eV.

III. RESULTS AND DISCUSSION

A. Ion energy distributions

Ion energy distributions are indicative of plasma characteristics such as the plasma potential, sheath width, and the operating pressure. In the case of collisionless sheaths, where the ion mean free paths are long compared to the sheath width, the ion energy distributions are narrow. In that case, ions will arrive at the electrode with energies equal to the sheath voltage, which is approximately equal to the plasma potential. Collisionless sheaths are typically found in high-density sources ($>10^{11}\,\mathrm{cm}^{-3}$) operated at low pressures ($<$20 mTorr), such as inductively coupled discharges. Ion energy distributions measured at the grounded electrode in inductively coupled discharges[8–10] exhibit narrow distributions [full width at half maximum (FWHM)$=$1–3 eV] centered about the plasma potential.

Measurements in the source region of the LAPPS discharge,[5] made under similar operating conditions, have found an electron temperature (T_e), plasma density (n_e), and plasma potential (V_p) of 1 eV, $2\times10^{11}\,\mathrm{cm}^{-3}$, and 2–3 V, respectively. Using these values we may estimate a Debye length, λ_D, of $\sim$10 μm and a sheath width[2,11] of a few λ_D. It is important to note that these lengths are a lower limit since n_e is found to decrease with distance from the discharge center. If we assume the ion-neutral cross section[12] is $6\times10^{-15}\,\mathrm{cm}^2$, we may estimate a mean free path of approximately 450 μm. From these estimates we conclude that the sheath should be nearly collisionless and the ion energy distributions should be indicative of such.

Previous investigators[7,9,13] have correctly pointed out that ion trajectories through small orifices can be altered if the presence of the orifice perturbs the local sheath potential. It has been suggested that the orifice diameter must be smaller than the sheath thickness[7] or even on the order of λ_D (Ref. 13) to minimize field distortions. The result of these field distortions is a broadening of the ion energy distribution toward the low energy side.[13] Given our estimates above, the orifice used in this work exceeds the minimum dimensions required to avoid distortions. As noted, however, these estimates are based on the source region measurements and should therefore represent the minimum λ_D. Furthermore, preliminary experiments using a smaller orifice have shown no change in the FWHM of the ion energy distributions and, as we will see, the most probable kinetic energy is in good agreement with the plasma potential. Because of these observations we contend that the kinetic energy distributions presented herein are a reasonable approximation to the true incident ion energy.

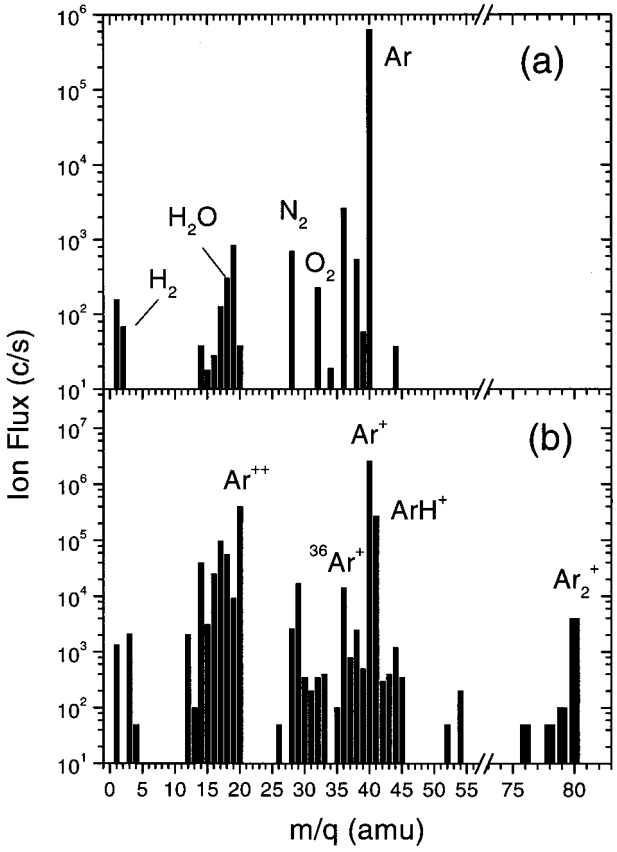

FIG. 4. (a) RGA mass spectrum of neutrals sampled from the reactor while at the operating pressure of 100 mTorr (no discharge). The neutral species are ionized by 35 eV electrons. (b) Mass distribution of ions sampled from the argon discharge. With the exception of Ar^{2+}, the energy of all ions sampled is 3.5 ± 0.5 eV, equal to the most probable Ar^+ energy according to Fig. 3. Because of its double charge, the energy of Ar^{2+} is twice that of single charged species.

Shown in Fig. 3 is the Ar^+ energy distribution for a source–electrode separation of 1 cm. For these experiments, $d=0$ cm is the edge of the electron beam defined by the edge of the slot in the anode. The distributions are measured during the pulse, from 0.2 to 1.0 ms, to only measure energies after the plasma reaches a steady state, i.e., to avoid effects from plasma ignition and decay. With the transmission energy set so that $\Delta E=0.3$ eV, the most probable kinetic energy is found to be $\approx$3.5 eV and the width of the distribution is $\approx$1 eV. This energy is in good agreement with the measured plasma potential[5] and with the calculated sheath potential.[2]

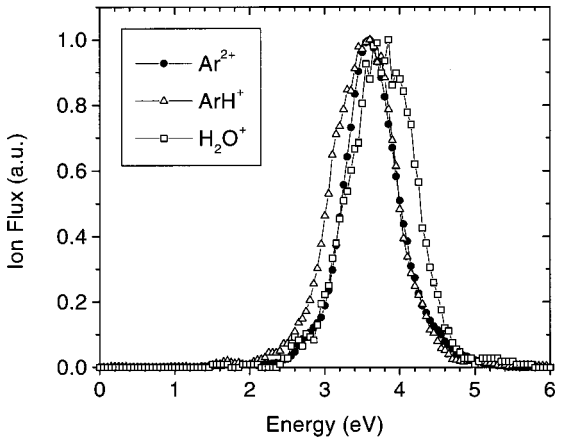

FIG. 5. Kinetic-energy distributions of Ar^{2+}, ArH^+, and H_2O^+ incident to the grounded electrode. The energy scale of the Ar^{2+} distribution has been halved. The electrode location and time resolution are identical to that in Fig. 3.

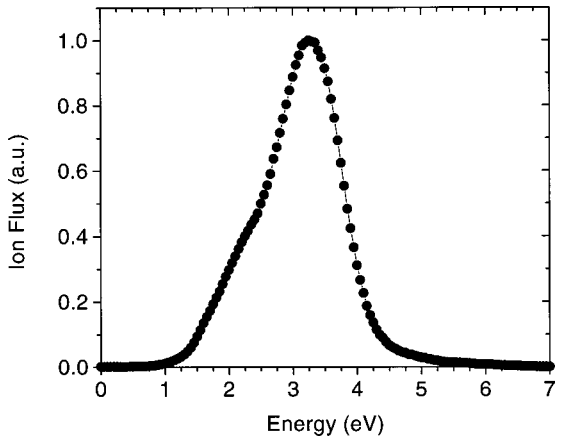

FIG. 6. Time-integrated kinetic-energy distribution of Ar^+ ions at the electrode surface. The location of the electrode is the same as that in Fig. 3 but the Ar^+ flux is sampled from 50 μs to 7 ms. Note the low-energy component of the distribution.

Shown in Fig. 4(b) is the mass spectrum of ions incident to the surface with the ion energy set to equal to the most probable Ar^+ energy of 3.5 eV. The transmission energy was increased for these measurements so that the effective energy window is ± 0.5 eV. For comparison, the RGA mass spectrum of neutrals sampled from the background (100 mTorr argon) is shown in Fig. 4(a). There are numerous ions present in the flux, some of which are related to background gas and others that are not. While a detailed discussion of the mechanisms leading to the observed ion flux is beyond the scope of this article, we note that in addition to direct (or dissociative) ionization by the high-energy electron beam, charge exchange with Ar^+ will also lead to ion production. For example, the reactions $Ar^+ + H_2O \rightarrow Ar + H_2O^+$ and $Ar^+ + H_2O \rightarrow ArH^+ + OH$ proceed at appreciable rates ($k \sim 10^{-9}$ cm^3/s).[14,15] At these rates and relative H_2O levels, we estimate the charge exchange mean free path to be on the order of centimeters, which explains the significant H_2O^+ and ArH^+ flux levels, which are not explained entirely by direct ionization.

Shown in Fig. 5 are the distributions for Ar^{2+}, ArH^+, and H_2O^+ using settings identical to those used in obtaining the Ar^+ distribution (Fig. 3). These distributions are similar to the distribution for Ar^+, suggesting that a majority of ions are created outside the sheath and thus experience the full sheath voltage. If the mean free path for charge exchange is comparable to the source–electrode separation but significantly greater than the sheath thickness, we would expect all ions to have similar distributions.

B. Time dependencies

Shown in Fig. 6 is a time-integrated Ar^+ energy distribution accumulated between 50 μs and 7 ms. In addition, the ion flux at a given energy was monitored as a function of time and is shown in Fig. 7. For these measurements, the EQP was set to pass a fixed energy ($E = \pm 0.25$ eV) and the output from the channeltron was monitored by a pulse counter. The pulse counter was configured to count pulses over a 10 μs gate which was then scanned over the entire measurement range. Each gate accumulates counts over at least 100 discharge pulses. Here, the ignition of the discharge defines $t = 0$ and the electron beam is extinguished at 1 ms. Note that the data are offset by the ion transit time in the EQP (≈ 70 μs).

In comparing the time-integrated distribution with the distribution taken only during the pulse (Fig. 3), a low-energy tail is apparent. Considering the time dependent nature of the ion flux, shown in Fig. 7, this low-energy tail is the result of ions incident to the surface after the electron beam is extinguished and the plasma slowly dissipates. The results suggest three general stages: ignition, steady state, and the postdischarge. The ignition is dominated by a flux of high-energy ions and the postdischarge is characterized by a flux of low-energy ions that persists for several milliseconds. During the steady state stage, the 4.0 eV ion flux decays while the 3.0

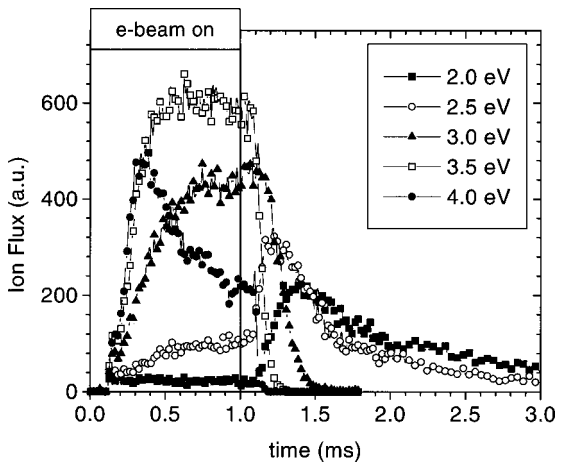

FIG. 7. Time- and energy-resolved Ar^+ flux measurements at the electrode surface located 1.0 cm from the electron beam. Argon ions of a selected energy (± 0.25 eV) are measured during a 10 μs time window that is scanned over the entire discharge and postdischarge periods. The low-energy flux in the postdischarge is attributed to the low-energy component in the distribution shown in Fig. 6.

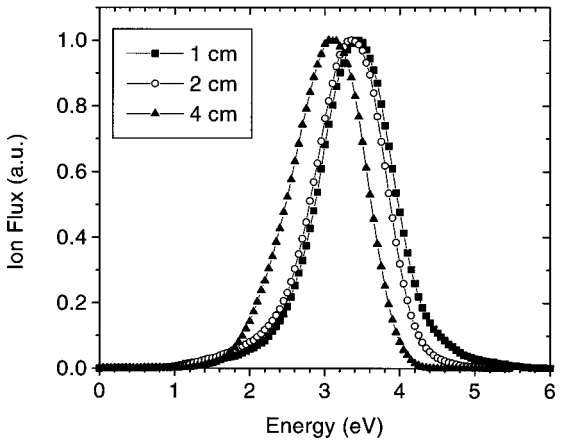

FIG. 8. Ar^+ kinetic-energy distributions collected during the plasma pulse (0.2–1.0 ms) for source–electrode separations of 1, 2, and 4 cm.

eV flux increases and the 3.5 eV flux remains nearly constant. Of course, the sum of these fluxes is nearly equivalent to the distribution seen in Fig. 3. Similar time dependencies have been observed in other pulsed sources.[16,17] Since the ion energy is related to V_p, it is reasonable to assume that the V_p (and thus T_e) follows similar time dependencies. Probe measurements[5] indicate a decreasing V_p and T_e in the postdischarge but a more careful study to correlate the observed ion flux with the V_p is needed to understand these time dependencies.

C. Distance dependencies

Shown in Fig. 8 are the Ar^+ distributions for a source–electrode separation of 1, 2, and 4 cm. Here again, the distributions are taken during the steady state phase of the discharge (0.2–1.0 ms). The widths are nearly identical for all distributions but the mean energy has decreased by approximately 0.5 eV at 4 cm. The Ar^{2+}, ArH^+, and H_2O^+ distributions exhibit similar features as Ar^+ and Fig. 9 gives the mean energy for all four species as a function of distance. Profiles of V_p and T_e as a function of distance from the source region indicate a decrease in both as the distance increases.[5] Here again, the correlation between the mean ion energy and V_p is evident.

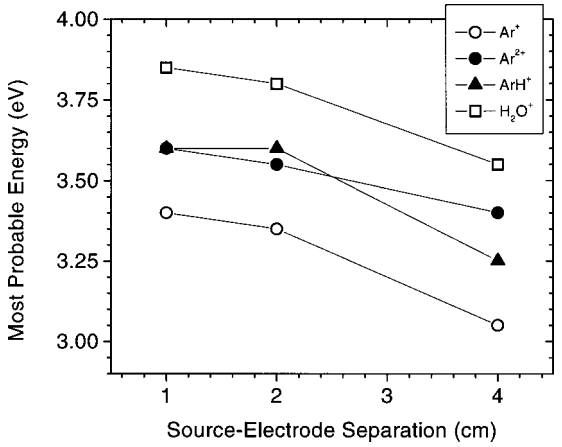

FIG. 9. Most probable ion energies for Ar^+, Ar^{2+}, ArH^+, and H_2O^+ at distances of 1, 2, and 4 cm from the source. Here again, the distributions are taken during the pulse and the uncertainty in energy is ± 0.15 eV.

IV. CONCLUSION

Mass resolved ion energy distributions, measured at a grounded electrode, exhibit features that are indicative of a pulsed, electron beam-generated plasma. The most probable ion kinetic energy is correlated to the plasma potential, which is found to have both temporal and spatial dependencies. The plasma, ion flux, and ion energy reach a steady state during the pulsed discharge. In the postdischarge, the flux and energies decrease and the low-energy flux persists for several pulse widths. In addition, ion energies are found to decrease with increasing source–electrode separation. Since the ion flux is measured at a grounded electrode, the incident ion energy should be approximately equal to the plasma potential. The ion energies suggest that the plasma potential is on the order of a few volts, in agreement with Langmuir probe measurements indicating electron beam-generated plasmas are characterized by low plasma potentials and electron temperatures. Further experiments are needed to better understand these distributions and their relationship to the fundamental plasma parameters.

ACKNOWLEDGMENTS

The authors greatly appreciate helpful conversations with Dr. Martin Lampe and Dr. Wallace Manheimer. Two of the authors (S.G.W. and D.D.B.) gratefully acknowledge support from the National Research Council. This work was supported by the Office of Naval Research.

[1] R. F. Fernsler, W. M. Manheimer, R. A. Meger, J. Mathew, D. P. Murphy, R. E. Pechacek, and J. A. Gregor, Phys. Plasmas **5**, 2137 (1998).
[2] W. M. Manheimer, R. F. Fernsler, M. Lampe, and R. A. Meger, Plasma Sources Sci. Technol. **9**, 370 (2000).
[3] K. D. Schatz and D. N. Ruzic, Plasma Sources Sci. Technol. **2**, 100 (1993).
[4] M. J. Kushner, W. Z. Collision, and D. N. Ruzic, J. Vac. Sci. Technol. A **14**, 2094 (1996).
[5] D. Leonhardt, S. G. Walton, D. D. Blackwell, W. E. Amatucci, D. P. Murphy, R. F. Fernsler, and R. A. Meger, J. Vac. Sci. Technol. A, these proceedings.
[6] J. W. Coburn and E. Kay, J. Vac. Sci. Technol. **8**, 738 (1971).
[7] J. Liu, G. L. Huppert, and H. H. Sawin, J. Appl. Phys. **68**, 3916 (1990).
[8] J. R. Woodworth, M. E. Riley, D. C. Meister, B. P. Aragon, M. S. Lee, and H. H. Swain, J. Appl. Phys. **80**, 1304 (1996).
[9] J. R. Woodworth, M. E. Riley, P. A. Miller, G. A. Hebner, and T. W. Hamilton, J. Appl. Phys. **81**, 5950 (1997).
[10] Y. Wang and J. K. Olthoff, J. Appl. Phys. **85**, 6358 (1999).
[11] M. A. Lieberman and A. J. Lichtenberg, *Principles of Plasma Discharges and Materials Processing* (Wiley, New York, 1994).
[12] E. W. McDaniel, *Collision Phenomena in Ionized Gases* (Wiley, New York, 1964).
[13] E. A. Edleberg, A. Perry, N. Benjamin, and E. S. Aydil, J. Vac. Sci. Technol. A **17**, 506 (1999).
[14] C. J. Howard, H. W. Rundle, and F. Kaufman, J. Chem. Phys. **53**, 3745 (1970).
[15] Z. Karpas, V. G. Anicich, and W. T. Huntress, Jr., Chem. Phys. Lett. **59**, 84 (1978).
[16] C. Charles and R. W. Boswell, J. Appl. Phys. **78**, 766 (1995).
[17] O. Zabeida, A. Hallil, M. R. Wertheimer, and L. Martinu, J. Appl. Phys. **88**, 635 (2000).